Supporting Information

Berke et al. 10.1073/pnas.1212186109

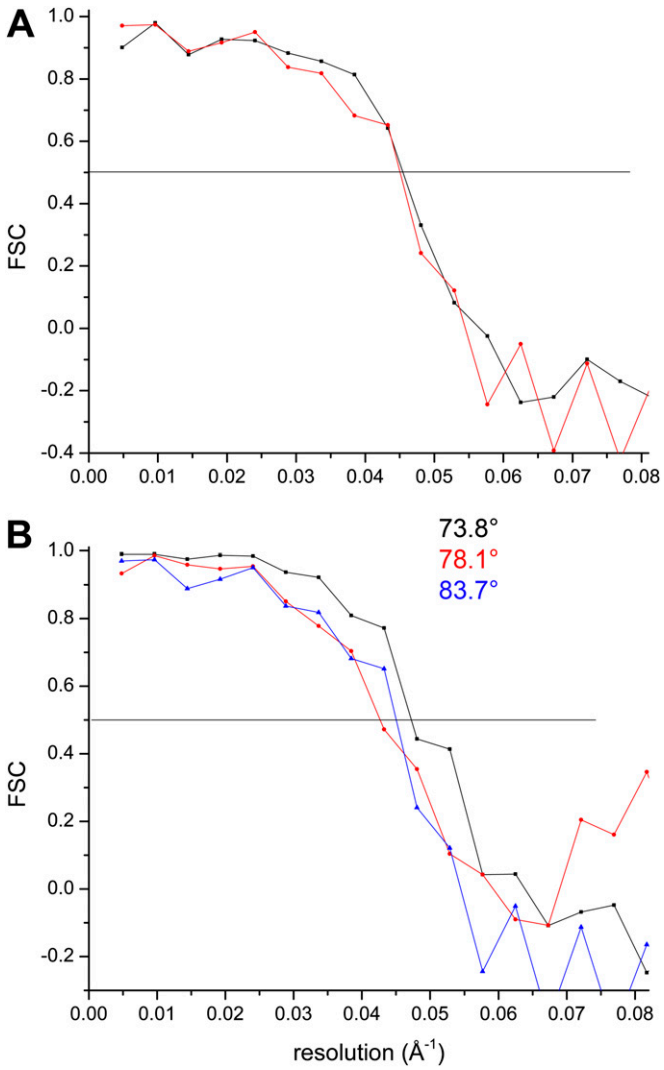

Fig. S1. Fourier shell correlation (FSC) plots. (*A*) FSC curves for the melanoma differentiation-associated protein 5 (MDA5)-dsRNA-ATP-γ-S filaments (black) and for the Δcaspase recruitment domain (ΔCARD)-MDA5-dsRNA-ATP-γ-S filaments (red). (*B*) FSC curves for three states of twist of the MDA5-dsRNA-ATP-γ-S filaments.

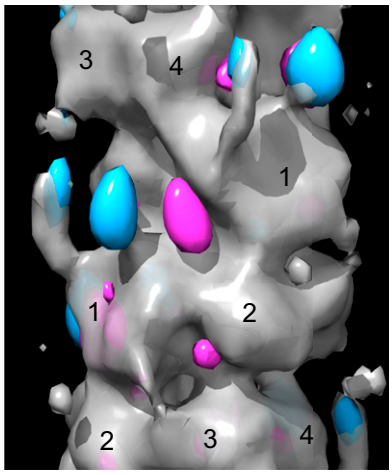

Fig. S2. Statistical difference map confirming the linkage position of the CARDs. The gray surface is the MDA5-RNA reconstruction displayed at a low threshold, with the four domains of density labeled 1–4 as in Fig. 1*F*. A difference map between this reconstruction and the ΔCARD-MDA5-RNA reconstruction is shown in cyan (positive density) and magenta (negative density), with these densities divided by the SE at each voxel. The SE was estimated by dividing each dataset into three datasets and determining the variance of the three different reconstructions for each of the two complexes (MDA5 and ΔCARD-MDA5). This avoids the problems encountered when estimating the variance from only two observations, which has a distribution (from the gamma function) with significant probability at very low values. The variance of the difference was taken as the sum of the variances of MDA5 and ΔCARD-MDA5. The differences are shown at a threshold of 5 σ. The cyan densities are where the MDA5 reconstruction is greater than the ΔCARD-MDA5 reconstruction, and the magenta densities are where the ΔCARD-MDA5 reconstruction is greater than the MDA5 volume. The two positive densities (cyan) are connected to domain 1, consistent with our contention that this is the Hel1 domain and that these positive densities in the difference map are the disordered CARD domains (and/or the CARD–Hel1 linker region). Given the 5 σ threshold, this difference is highly significant ($P < 0.001$). In addition, a significant negative density (magenta) is associated with domain 1 at a smaller radius, which may arise from a conformational change. On the other hand, we needed to impose the twist of the MDA5 reconstruction (87.0°) on the MDA5-ΔCARD reconstruction (83.7°), so some component of this negative density may be an artifact.

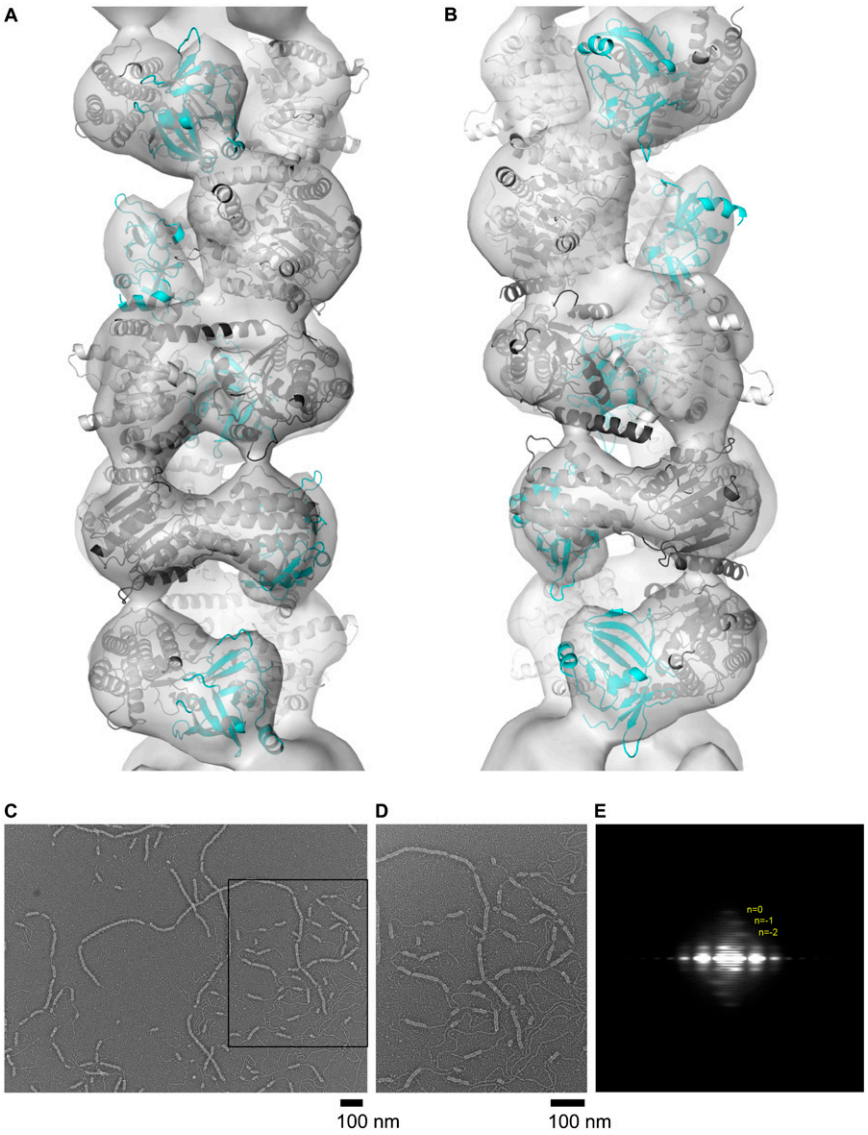

Fig. S3. Comparison of the fit of the MDA5 homology model into the two enantiomers of the MDA5-dsRNA-ATP-γ-S filament reconstruction. (*A*) With the enantiomer that gives the best fit (0.96 correlation), only minor structural elements are outside the EM density. The helical rise of the protein is right-handed (Fig. 2*B*). (*B*) With the other enantiomer (0.92 correlation), the helix bridging the Hel1 and Hel2 domains lies outside EM density (dark gray, center). (*C*) Fast-freeze, deep-etch micrograph of MDA5-dsRNA filaments. (*D*) Magnification of *C Inset*. Regions of naked dsRNA are visible emerging from thicker MDA5 filaments. (*E*) Averaged power spectrum of filaments from fast-freeze, deep-etch micrographs confirming the right-handed helical twist. Power spectra were generated from 688 nonoverlapping segments, each 100 pixels long (7.5 Å/pixel), and averaged together. F-actin was coprepared with the MDA5 filaments, with the 59-Å pitch left-handed actin helix used as a control to ensure that the absolute hand of the images was correct.

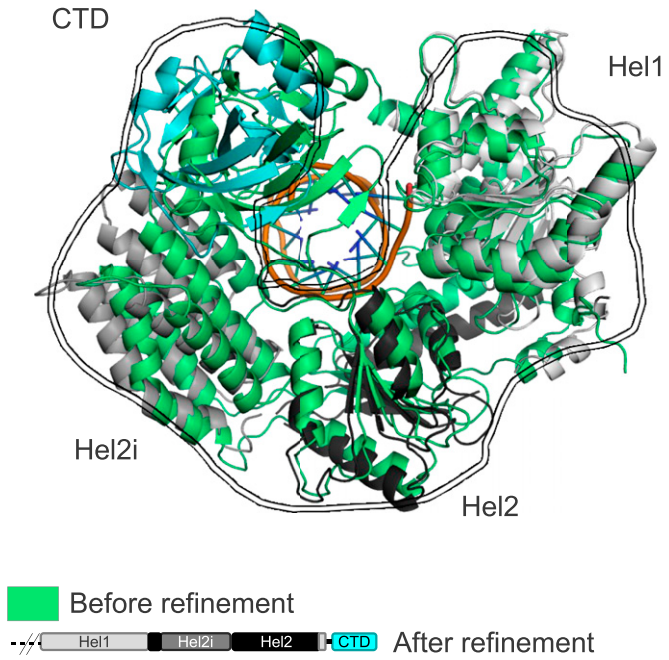

Fig. S4. Domain motions associated with rigid body refinement. Positional refinement of the MDA5 domains Hel1, Hel2, Hel2i, and C-terminal domain (CTD) as rigid bodies resulted in shifts of all four domains away from the axis of the filament. The CTD underwent the largest shift, moving into the domain 4 density and resolving a clash with the RNA present in the retinoic acid-inducible gene 1 (RIG-I)–based homology model before refinement. The double line represents the outline of an EM density section at the center of the MDA5 molecule.

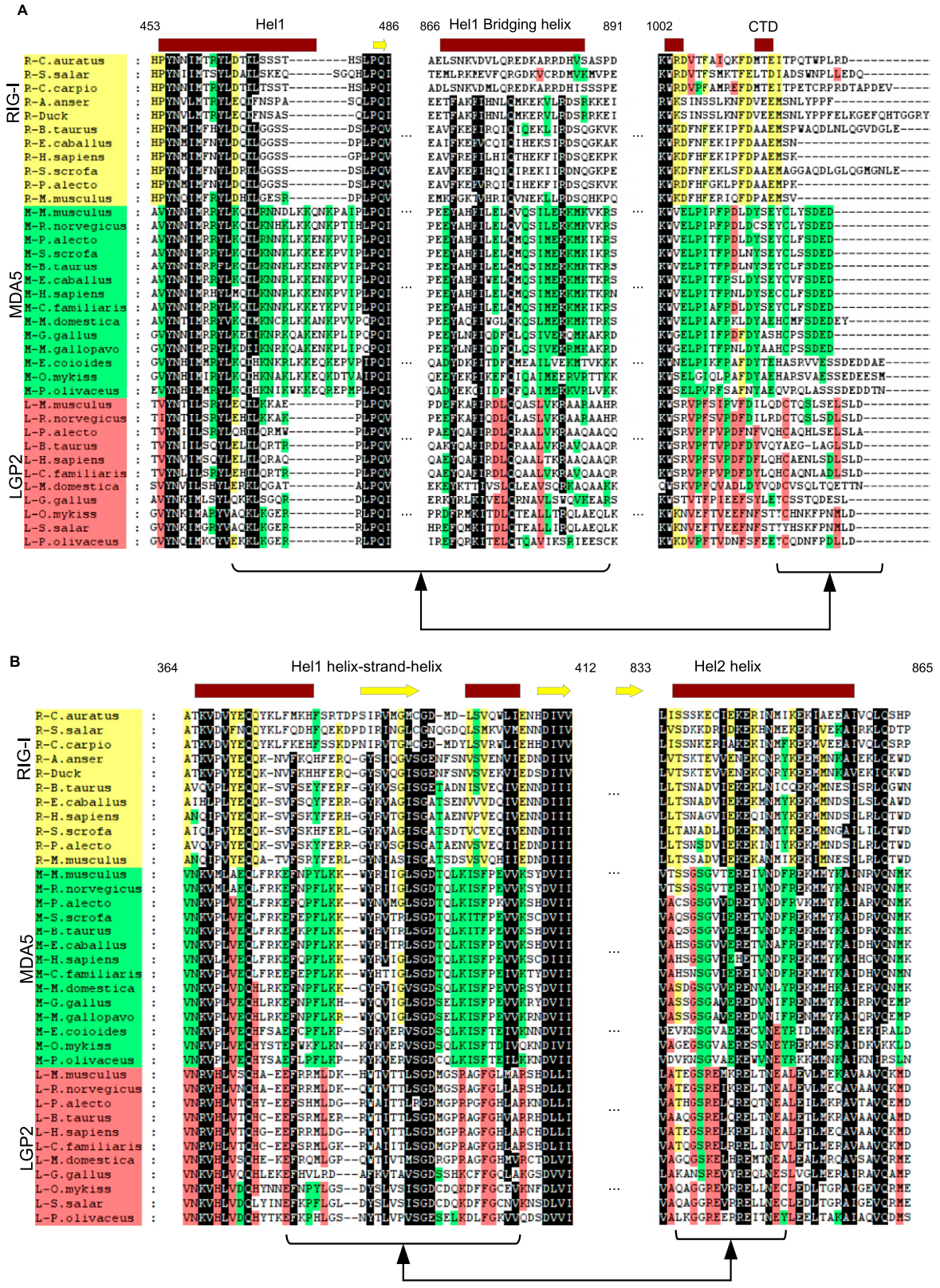

Fig. S5. Amino acid sequence alignments of MDA5, RIG-I, and LGP2 from various vertebrate species. (*A*) Sequences of the Hel1 and Hel1 bridging helix and CTD regions involved in Hel1–CTD interring contacts in the MDA5 filament model (Fig. 2*C*). The C terminus of the CTD is conserved across species in MDA5, but is significantly different in RIG-I and LGP2. (*B*) Sequences of the Hel1 and Hel2 regions involved in Hel1–Hel2 interring contacts in the MDA5 filament model (Fig. 2*D*). The numbers at the top refer to the mouse MDA5 sequences. Predicted or known secondary structures for MDA5 are indicated (red box, α-helix; yellow arrow, β-strand).

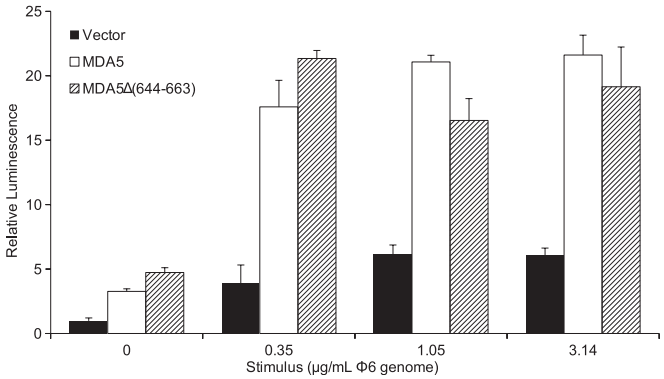

Fig. S6. MDA5-dependent signaling in response to genomic dsRNA from bacteriophage Φ6. HEK293T cells were transfected with firefly luciferase under control of the IFN-β promoter and vector only, WT human MDA5, or human MDA5-Δ(644-663). After expression for 24 h, cells were transfected with genomic dsRNA from Φ6 at the indicated concentrations. After 16 h, cell lysates were prepared, and luciferase activity was measured. Similar levels of IFN signaling in response to Φ6 RNA were observed with the two MDA5 constructs, but not with the vector-only negative controls. Firefly luciferase activity was normalized to cotransfected *Renilla* luciferase under a constitutive promoter (n = 3; mean ± SD).

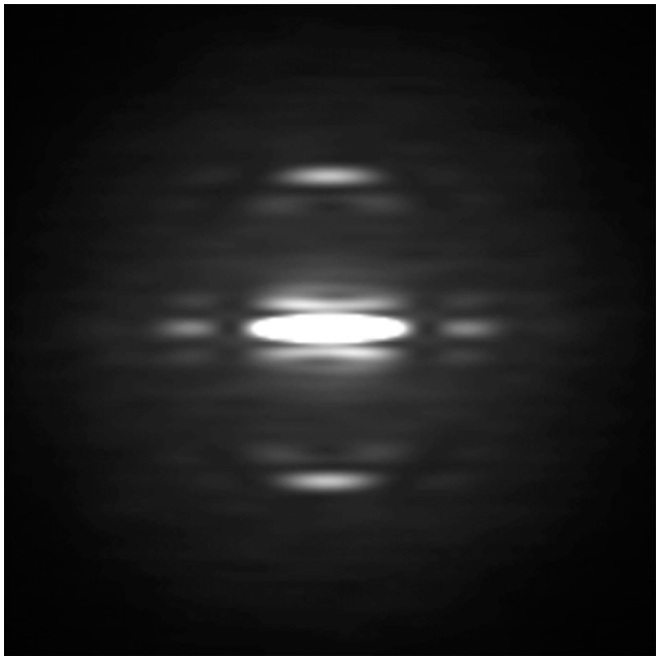

Movie S1. Animation showing in sequence the power spectra from three different mean states of twist. Differences in the power spectra explain why the layer lines other than the strong meridional reflection are blurred out in a global average. These three power spectra were generated from classes with a mean twist of 73.8°, 78.1°, or 83.7° between adjacent rings. There was no evidence of discrete twist states, and grouping into three classes was arbitrary.

Movie S1

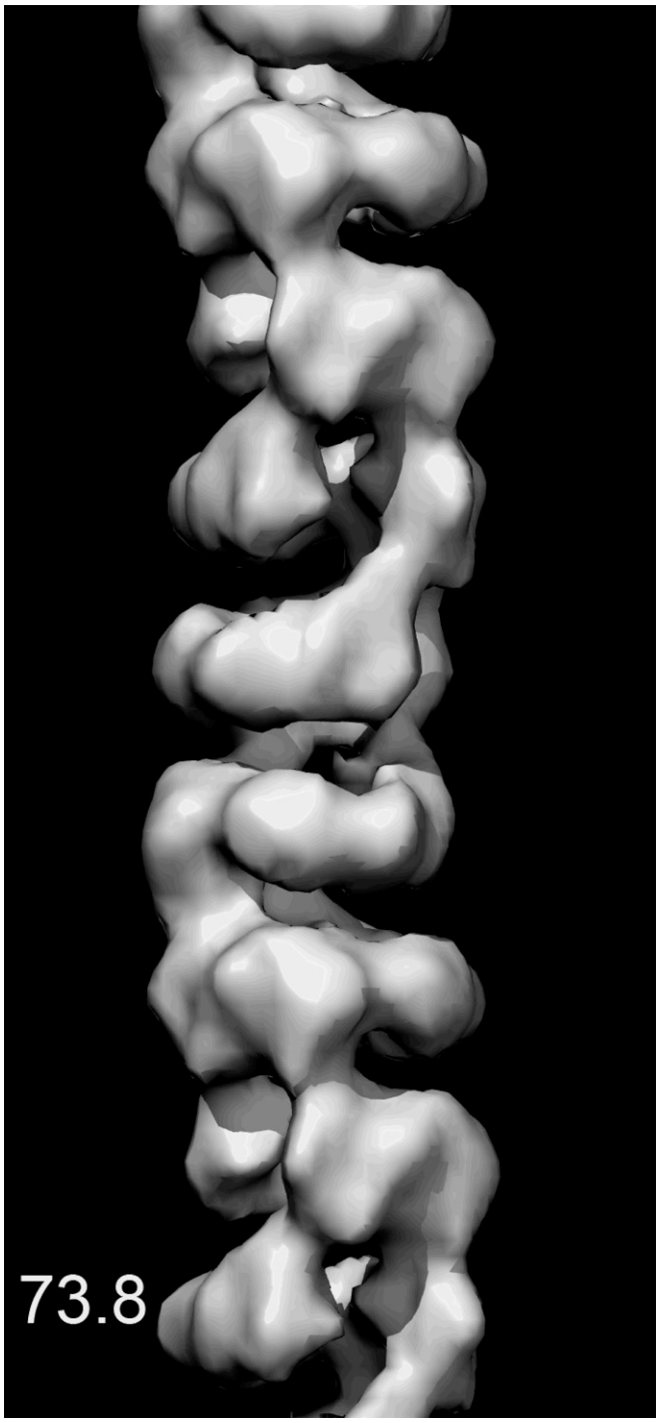

Movie S2. Animation showing in sequence the superimposed reconstructed EM volumes of the MDA5-dsRNA-ATP-γ-S filament generated from classes characterized with a mean twist of 73.8°, 78.1°, or 83.7° between adjacent MDA5 rings. Given the variability of these volumes, any small nucleotide-dependent changes in the filament structure would not be expected to be readily detectable.

Movie S2